Springer

KSME

Journal of Mechanical Science and Technology 32 (1) (2018) 465~479
www.springerlink.com/content/1738-494x(Print)/1976-3824(Online)
DOI 10.1007/s12206-017-1248-0

A strong tracking filter based multiple model approach for gas turbine fault diagnosis †

Qingcai Yang, Shuying Li and Yunpeng Cao*

College of Power and Energy Engineering, Harbin Engineering University, Harbin 150001, China

(Manuscript Received March 29, 2017; Revised July 28, 2017; Accepted September 13, 2017)

Abstract

In this paper, a nonlinear Fault detection and isolation (FDI) based on an improved Multiple model (MM) approach was proposed for the gas turbine engine. A bank of Strong tracking extended Kalman filters (STEKFs) was designed that enables robustness to model uncertainty and overcomes the shortcoming of the MM approach. The Jacobian matrix used in the filters was deduced by using the non-equilibrium analytic linearization method to improve the traditional method. Hierarchical fault detection and isolation architecture based on evaluating the maximum probability criteria were developed for both single and multiple faults. In addition, a nonlinear mode set automatic generation method that enables automatic generation of the modes of each level in the hierarchical architecture was also presented. Fault detection and isolation of a two-shaft marine gas turbine was studied in a simulation environment using the proposed STEKF-based MM approach and compared with the results of the traditional Extended Kalman filter (EKF) based MM approach. The results showed that the proposed approach not only has the advantages of the EKF-based MM approach but also robustness to the model uncertainty and overcomes the shortcomings of the MM approach.

Keywords: Gas turbine engine; Gas path fault; Fault detection and isolation; Multiple model approach; Strong tracking extended Kalman filter

1. Introduction

The gas turbine engine, as important power machinery, undergoes unavoidable failure with increase of service time. The gas path fault, as the most common fault in the gas turbine engine, has been widely studied by researchers. The main causes of gas path fault include fouling, erosion, corrosion and Foreign object damage (FOD). These causes will result in performance degradation of the gas turbine engine, further reduce its safety and stability, and lead to increase fuel consumption as well as operation and maintenance cost [1, 2]. Fault diagnosis of gas turbines plays an important role in improving the reliability and reducing the operation and maintenance costs of the gas turbine engine. It can detect the occurrence and locate the fault in time to prevent a catastrophe and then contribute to the development of a maintenance schedule. Fault detection and isolation (FDI), as the core of gas turbine fault diagnosis, has received extensive attention from researchers in recent years. On the one hand, the FDI of complex nonlinear systems such as gas turbines engine is more complicated than that of linear systems. On the other hand, sophisticated FDI algorithms do not necessarily result in a more accurate diagnosis [3].

In the past few decades, researchers have proposed a variety of FDI methods. These methods are developed on the basis of Gas path analysis (GPA), which can detect and isolate gas turbine faults by observing the deviation in engine measurement parameters such as rotational speed, pressure, temperature, and fuel flow [4]. Based on the available knowledge of the gas turbine, FDI can be categorized into three main approaches, namely, model-based [5], data-driven [6] and expert system [7]. The model-based approach, as one of the most widely used fault diagnosis approach, allows one to represent all prior knowledge of the gas turbine as a mathematical model and then accomplish the objective of FDI through the mathematical model and measured data of the gas turbine. The estimation method, as the most popular model-based approach, is widely used in gas turbine online fault detection and isolation due to its real-time property.

A variety of estimation algorithms have been proposed, such as the Kalman filter and its derivative method [8-10] and the particle filter method [11]. The complexity of different FDI methods causes their performance and computational cost to differ, but the more complex the algorithm, the higher the computation cost. Therefore, it is necessary to trade off the accuracy and the computational cost of on-line gas turbine fault detection and isolation. A method named the Multiple

*Corresponding author. Tel.: +86 45182569647, Fax.: +86 45182560595
E-mail address: caoyunpeng@hrbeu.edu.cn
† Recommended by Associate Editor Tong Seop Kim

model (MM) based FDI approach can simultaneously ensure high accuracy and reasonable computational cost. The MM-based FDI is based on a conditional hypothesis, which transforms the complex fault detection and isolation problems into pattern recognition problems. Several modes that represent the possible operating conditions of the gas turbine will be established, and a bank of Kalman filters, which correspond to these modes, is designed to recognize the mode that matches the current operating condition. Thus, the filter estimation residual of the mode that matches the current operating condition will be close to zero, whereas the other filters will have a significant estimation residual. Therefore, the fault can be detected and isolated via the mode that with the minimum estimation residual in the bank of filters.

In Ref. [12], the Multiple model adaptive estimation (MMAE) method is applied to detect the sensor and actuator faults in an aircraft engine control system. Both single and dual sensors as well as actuator faults are addressed. Moreover, a hierarchical architecture is used to reduce the number of filters and improve the computational efficiency. In Ref. [13], the Residual correlation Kalman filter bank (RCKFB) based on the MMAE algorithm is proposed to detect the actuator fault of the control system in the turboshaft engine. In Ref. [14], the MM-based FDI approach is used for the first time to detect and isolate the gas path fault of the gas turbine, and a modular and hierarchical architecture is developed that enabled the detection and isolation of both single and concurrent multiple faults in the jet engine. In addition, the effect of sensor failure and the extensive levels of noise outliers in the sensor measurements are analysed. Then, the Extended Kalman filter (EKF) and the Unscented Kalman filter (UKF) based MM approach are proposed [15]. This study shows that considerable performance improvements could be accomplished by the UKF over the EKF and that the UKF is significantly more robust to large sensor noise.

The choice of the filter has a great influence on the performance of the MM-based FDI approach. Although the computational cost of the linearized Kalman filter is low, but the gas turbine is a nonlinear system, so it will have a large estimation error. Furthermore, the UKF needs to choose $2n+1$ sigma points, which greatly increases the computational cost, so it may not be suitable for on-line fault detection and isolation applications. While the EKF as a nonlinear estimation method has a reasonable computational cost and more widely used. However, the EKF has poor robustness to model uncertainty and sensor noise [16]. For the model-based fault detection and isolation approach, model uncertainty exists due to the model simplification and the inaccurate initial noise covariance matrices. In addition, the EKF needs to linearize the nonlinear model around the Kalman filter estimate, so the model uncertainties will be further increased. Therefore, the EKF may diverge due to the presence of model uncertainty and large sensor noise, which affects the MM-based FDI results.

In addition, the design of the mode set is another important part of the MM-based FDI approach. The mode set needs to include all possible operating conditions of the gas turbine. It is acquired in advance and then selected according to the previous results in the existing approach [14], which will be difficult to apply practically. Moreover, in the MM-based FDI approach, the hypothesis conditional probability of each mode is recursively calculated by using Bayes' law. However, due to the model uncertainty and large sensor noise, the difference between modes will be reduced so that too unobvious to distinguish. This will affect the performance of the MM-based FDI approach. Furthermore, the hypothesis conditional probabilities of each mode are obtained through the Gaussian density function. This means that the filter residuals of each mode should follow the Gaussian distribution, but it is usually not satisfied in practice.

Therefore, in this paper, an improved MM-based nonlinear FDI approach was proposed to overcome the problems mentioned above. A bank of Strong tracking extended Kalman filter (STEKF) was designed for a nonlinear dynamic model of the two-shaft marine gas turbine. The STEKF uses the orthogonality principle and the suboptimal fading factor to forcing filter residual has orthogonality or approximate orthogonality. It has the advantages of robustness to model uncertainty and insensitivity to sensor noise [16]. In addition, the generalized Jacobian matrix used in the STEKF was deduced using the non-equilibrium analytic linearization method. It is overcome the shortcomings of the traditional method that obtaining the Jacobian matrix by calling the gas turbine nonlinear model multiple times, so that the Jacobian matrix used in the STEKF can be calculated in real time.

In addition, the STEKF-based MM approach was implemented for the two-shaft marine gas turbine and tested in a simulation environment. A hierarchical architecture that enables the detection and isolation of both single faults and multiple faults in the gas turbine was developed. The mode set of each level in the hierarchical architecture was generated automatically according to the detection and isolation results of the previous level by using the mode set automatic generation algorithm. In this algorithm, the fault factors are regard as control variables, and the corresponding fault modes are generated by changing the value of the fault factors. Finally, the results of the proposed STEKF-based MM approach was compared with those of the traditional EKF-based MM approach.

The remainder of this paper is organized as follows: Sec. 2 briefly describes the nonlinear dynamic model of the gas turbine studied in this paper. The STEKF-based MM approach is described in detail in Sec. 3. Sec. 4 deduces the generalized Jacobi matrix used in the STEKF by using the non-equilibrium point analytic linearization method, and the generalized model of the mode set is obtained. In Sec. 5, the hierarchical fault detection and isolation architecture is developed, and the mode set automatic generation method is presented; then, both the single fault and multiple faults are detected and isolated in the simulation environment. Sec. 6 analyses and

discusses the results of the proposed STEKF-based MM approach and compares it with the results of the EKF-based MM approach. The conclusions of this paper are presented in Sec. 7.

2. Nonlinear dynamic model of a gas turbine engine

In this section, the nonlinear dynamic model of the gas turbine will be described briefly. This paper mainly studies the fault detection and isolation of a two-shaft marine gas turbine engine, the main components of the gas turbine include the compressor, combustion chamber, compressor turbine and power turbine. A schematic diagram of the gas turbine engine shows in Fig. 1, where the propeller and reduction gearbox are simplified as a load.

The nonlinear dynamic model of the engine was developed in the environment of MATLAB/Simulink based on a previous work [17]. Considering the rotor dynamics and the volume dynamics, the main differential equations of the engine model are shown in Eq. (1). A more detailed description of the model can be found in Refs. [18-20]. The gas turbine considered in this paper is a marine gas turbine whose load has a cubic relationship with the propeller speed which linearly related to the power turbine speed. Therefore, the load power was expressed as a cubic relationship with the power turbine rotational speed.

$$
\begin{aligned}
\dot{N}_1 &= [\frac{30}{\pi}]^2 \frac{1}{J_1 N_1}[m_{CT}\eta_m c_{pg}(T_3 - T_4) - m_C c_p (T_2 - T_1)] \\
\dot{N}_2 &= [\frac{30}{\pi}]^2 \frac{1}{J_2 N_2}[m_{PT} c_{pg}(T_4 - T_5) - \Phi N_2^3] \\
\dot{T}_3 &= \frac{R_g T_3}{P_3 V_1 c_{vg}}[k(c_{pg} T_2 m_C + LHV \eta_{CC} w_f - c_{pg} T_3 m_{CT}) - \\
&\quad c_{pg} T_3 (m_C + w_f - m_{CT})] \\
\dot{P}_3 &= \frac{P_3}{T_3}\dot{T}_3 + \frac{R_g T_3 (m_C + w_f - m_{CT})}{V_1} \\
\dot{P}_4 &= \frac{(m_{CT} - m_{PT}) R_g T_4}{V_2} \\
\dot{P}_5 &= \frac{(m_5 - \Gamma\sqrt{P_5}) R_g T_5}{V_3}
\end{aligned}
\tag{1}
$$

where η_m is the mechanical efficiency, J_1 and J_2 are the inertia of the compressor shaft and power turbine shaft, respectively, Φ is the relationship coefficient between the power turbine rotational speed and the load power, LHV is the fuel low heating value, V_1, V_2 and V_3 are the component volumes, and Γ is the relationship coefficient between mass flow and pressure. The subscripts C, CT, PT, CC and g indicate the compressor, compressor turbine, power turbine, combustion chamber and gas, respectively.

Typical causes of gas turbine fault include fouling, erosion, corrosion, and Foreign object damage (FOD). These faults result in a change in the corrected mass flow (m) and the isentropic efficiency (η) of the components. In this paper, we only considered the faults that will cause m and η decrease. Therefore, six kinds of faults were investigated in this paper, as shown in Table 1. In this table, F denotes the fault factor, which equals to 1 when gas turbine in a healthy condition and between 1 and 0 when the fault occurs. For instance, $F_{mc} < 1$ indicates that a compressor fault occurs and causing the compressor corrected mass flow decrease.

Table 1. Component fault and its description.

Effect of component fault	Description
Change in compressor corrected mass flow	ΔF_{mc}
Change in compressor isentropic efficiency	$\Delta F_{\eta c}$
Change in compressor turbine corrected mass flow	ΔF_{mct}
Change in compressor turbine isentropic efficiency	$\Delta F_{\eta ct}$
Change in power turbine corrected mass flow	ΔF_{mpt}
Change in power turbine isentropic efficiency	$\Delta F_{\eta pt}$

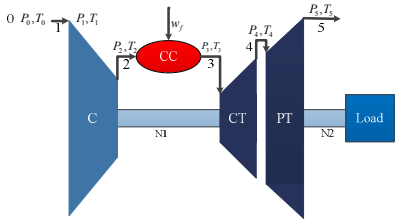

Fig. 1. Schematic diagram of the two-shaft marine gas turbine.

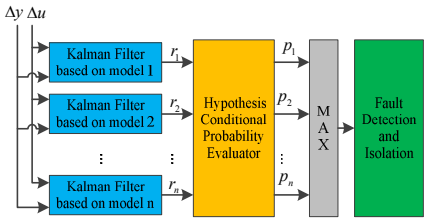

Fig. 2. General architecture of the MM-based FDI approach.

3. The STEKF-based multiple model approach

Fig. 2 shows the general architecture of the MM-based FDI approach [21]. In this architecture, a mode set that represents the possible operating conditions (Namely, healthy and different faulty conditions) of the gas turbine is obtained, and then, a bank of Kalman filters is designed corresponding to each mode in the mode set. For the bank of filters, given a set of measurement parameters y and control variable u, each filter will produce a filter residual vector r_i. Because each mode represents a possible operating condition of the gas turbine, the filter residual of each filter will be different. The filter residual of the mode that consistent with the current operating condition will be close to zero, and the residual of the other modes will be large. Hence, these filter residuals represent the approximation of each mode and the current operating condition of gas turbine. Therefore, according to these filter residu-

als, the hypothesis conditional probability evaluator will recursively calculate the conditioned probability of each mode by using Bayes' law, and the sum of conditional probabilities for these modes is always 1. Thus, the higher probability of the mode, it is more likely to be consistent with the current operating condition, so the mode can be detected and isolated by using the maximum probability criteria.

3.1 Strong tracking extended Kalman filter

The STEKF is derived from the EKF, which introduces the suboptimal fading factor into the estimation error covariance matrix of the EKF. The role of the suboptimal fading factor is to adjust the gain matrix in real time, and the forcing filter residual has orthogonality or approximate orthogonality. The STEKF has the following advantages: strong robustness against model uncertainties and very good real-time state tracking ability even when there is a state jump, regardless of whether the system has reached a steady state [16]. The STEKF will be introduced briefly in this section.

A discrete-time nonlinear system is shown in Eq. (2):

$$\begin{aligned} x_k &= f(x_{k-1}, u_{k-1}) + w_{k-1} \\ y_k &= h(x_{k-1}) + v_{k-1} \end{aligned} \tag{2}$$

where x is the state variable, u is the control variable, y is the measurement, and w and v are the process noise and the measurement noise, respectively. These noises are assumed to be a zero-mean Gaussian noise and the covariance is Q and R, respectively.

Introducing the suboptimal fading factor into the estimation error covariance matrix (P_k) and assuming the factor is λ_{k-1}, the modified P_k can be obtained as:

$$P_k = \lambda_{k-1} A P_{k-1}^{+} A^T + Q \,. \tag{3}$$

The suboptimal fading factor can be recursively solved by Eq. (4):

$$\begin{aligned} &E[(x_k^+ - \hat{x})(x_k^+ - \hat{x})^T] = \min \\ &E[(y_k)^T (y_{k+1+j})] = 0, k = 0,1,2,..., j = 1,2,... \end{aligned} \tag{4}$$

The second equation of Eq. (4) is called the orthogonality principle, whose physical meaning is that the residual error series should be made mutually orthogonal at each step, and it makes the filter robust to the uncertainty of the model. The STEKF algorithm is shown in Table 2, and more detailed information can be found in the Ref. [16].

The STEKF overcomes the shortcomings of the traditional EKF, so the STEKF-based MM approach will has better robustness to the model uncertainty than the EKF-based MM approach. Meanwhile, it will force the filter residuals follow the normal distribution and satisfy Bayes' law. However, the MM-based FDI approach is a model-based approach and usually requires a sufficiently difference between models, while the STEKF has a "Smoothing" effect on model. The "Smoothing" effect on models result in the difference between models will not significant, which makes fault detection and isolation more difficult. To solve the problem mention above, an effec-

Table 2. The STEKF algorithm.

The prediction step
$\hat{x}_k = f(\hat{x}_{k-1}^+, u_{k-1})$
$P_k = \lambda_{k-1} A P_{k-1}^+ A^T + Q$
The measurement update step
$K_k = P_k C^T (C P_k C^T + R)^{-1}$
$S_k = C(A P_{k-1}^+ A^T + Q) C^T + R$
$\gamma_k = y_k - h(\hat{x}_k)$
$\hat{x}_k^+ = \hat{x}_k + K_k \gamma_k$
$P_k^+ = (I - K_k C) P_k$
$\lambda_k = \begin{cases} \lambda_0, & \lambda_0 \geq 1 \\ 1, & \lambda_0 < 1 \end{cases}$
$\lambda_0 = \dfrac{tr[N_k]}{tr[M_k]}$
$N_k = V_k^0 - C Q C^T - \beta R$
$M_k = C A P_{k-1}^+ A^T C^T$
$V_k^0 = \begin{cases} \gamma_1 (\gamma_1)^T, & k = 0 \\ \dfrac{\rho V_{k-1}^0 + \gamma_k (\gamma_k)^T}{1+\rho}, & k \geq 1 \end{cases}$
Notation
$A = \dfrac{\partial f(\hat{x}_{k-1}^+, u_{k-1})}{\partial x}$
$C = \dfrac{\partial h(\hat{x}_k)}{\partial x}$
$tr[\cdot]$ *denotes the trace of a matrix*
ρ *denotes forgetting factor*
β *denotes softening factor*

Table 3. The EKF algorithm.

The prediction step
$\hat{x}_k = f(\hat{x}_{k-1}^+, u_{k-1})$
$P_k = A P_{k-1}^+ A^T + Q$
The measurement update step
$K_k = P_k C^T (C P_k C^T + R)^{-1}$
$S_k = C P_k C^T + R$
$\gamma_k = y_k - h(\hat{x}_k)$
$\hat{x}_k^+ = \hat{x}_k + K_k \gamma_k$
$P_k^+ = (I - K_k C) P_k$
Notation
$A = \dfrac{\partial f(\hat{x}_{k-1}^+, u_{k-1})}{\partial x}$
$C = \dfrac{\partial h(\hat{x}_k)}{\partial x}$

tive solution approach was used in this paper. When updating the model probability, the traditional EKF was used to calculate the filter residuals and the covariance matrix of the filter residuals. The suboptimal fading factor was introduced during the filtering and state estimation so that the above-mentioned problem can be addressed effectively. To evaluate the performance of the method proposed in this paper, it was compared with the traditional EKF method. The EKF algorithm is shown in Table 3, and detailed information can be found in Ref. [5].

3.2 Hypothesis conditional probability

In the MM-based FDI approach, the mode set represents all possible current conditions of the gas turbine, including healthy and different faulty conditions. At a given discrete time k, each filter will produce a filter residual vector, which represents the approximation of each mode and the current operating condition of gas turbine. The hypothesis conditional probability was used to represent the approximation of these modes and the current condition. Hypothesis conditional probability $p_i(k)$ is defined as the probability that the gas turbine operating condition is m_i ($i = 1, 2 \ldots n$ denotes the number of the modes) when given a measurement vector y_k at discrete time k, that is:

$$p_i(k) = \Pr[m = m_i \,|\, y(t_k) = y_k]\,. \tag{5}$$

The hypothesis conditional probability at a given time k of all modes can be recursively calculated from the values at time k-1 and the conditional probability densities for the current measurement y_k, as shown in Eq. (6):

$$p_i(k) = \frac{f_z(y_k \,|\, i, y_{k-1}) p_i(k-1)}{\sum_{j=1}^{n} f_z(y_k \,|\, j, y_{k-1}) p_j(k-1)} \tag{6}$$

where $f_z(y_k|i,y_{k-1})$ denotes the conditional probability density of the *i-th* mode when the measurements is y_k and $p_i(k\text{-}1)$ denotes the hypothesis conditional probability of the *i-th* mode at time k-1. The Gaussian conditional probability density function is shown in Eq. (7).

$$f_{y(t_k)|m_j, y(t_{k-1})}(y_k \,|\, m_j, y_{k-1}) = \frac{1}{(2\pi)^{m/2} |S_j|^{1/2}} \exp[\frac{1}{2} v_j^T S_j v_j] \tag{7}$$

where m is the dimension of the measurement parameters, S_j is the innovation vectors, and v_j is the filter's residual vectors, and these vectors can be obtained in the filtering process.

3.3 Fault detection and isolation logic

By comparing the hypothesis conditional probabilities of these modes that represent the possible operating conditions of gas turbine, it is possible to detect and isolate the fault of the gas turbine. If the current operating condition of the gas turbine is consistent with the *j-th* mode m_j, then the filter residual of mode m_j will be close to zero, so the corresponding conditional probability densities will be close to maximum. Meanwhile, the filter residuals of the other modes are larger than that of mode m_j, and the conditional probability densities are smaller than that of mode m_j. According to Eq. (6), with recursively calculation, the hypothesis conditional probability of mode m_j will increase until close to 1, while the hypothesis conditional probability of the other modes will decrease until close to 0. Therefore, the maximum probability criteria can be used to detect and isolate the fault, as shown in Eq. (8).

$$j = \arg \max_{i=1 \ldots n} p_i(k) \tag{8}$$

where j represents the *j-th* mode that is consistent with the current operating condition of the gas turbine.

4. Jacobian matrix determination based on analytic linearization

The STEKF estimation accuracy and computational cost depend on the calculation frequency of the Jacobian matrix. However, the calculation of the Jacobian matrix of the gas turbine nonlinear dynamic model is complicated, so some methods have been proposed, such as periodic updates or direct calculation offline, but they will increase the estimate error [9]. In addition, the MM-based FDI approach used in this paper needs to design a bank of filters, so it will have a large computational cost if using the existing methods. To overcome these problems, in this paper, the non-equilibrium analytic linearization method was used to derive a generalized analytic expression for the Jacobian matrix under the non-equilibrium point.

4.1 Non-equilibrium linearization

The engine model as shown in Eq. (1) is a nonlinear system as shown in Eq. (9). The elements of the vector F are equal to 1 when the gas turbine is in healthy condition, and at least one element is less than 1 when a fault occurs.

$$\begin{aligned} \dot{x} &= f(x, F, u) + w \\ y &= h(x, F) + v \end{aligned} \tag{9}$$

where x denotes the state variable, $x = [N_l, N_p, T_3, P_3, P_4, P_5]^{\mathrm{T}}$; u denotes the control variable, $u = w_f$; y denotes the output variable, $y = [\, N_l, N_p, T_2, P_2, T_4, P_4, T_5, P_5]^T$; F denotes fault factors, $F = [F_{mc}, F_{\eta c}, F_{mcT}, F_{\eta cT}, F_{mpT}, F_{\eta pT}]^T$.

At arbitrary point (x_i, F_i, u_i), a Taylor expansion was performed on Eq. (9), and the high order terms were ignored. A linearization model as shown in Eq. (10) can be obtained [22]:

$$\begin{aligned} \dot{x} &= f(x_i, F_i, u_i) + L_i \Delta x + M_i \Delta F + N_i \Delta u \\ y &= h(x_i, F_i) + E_i \Delta x + H_i \Delta F \end{aligned} \tag{10}$$

where

$$L_i = \frac{\partial f}{\partial x}(x_i, F_i, u_i), M_i = \frac{\partial f}{\partial F}(x_i, F_i, u_i), N_i = \frac{\partial f}{\partial u}(x_i, F_i, u_i)$$

$$E_i = \frac{\partial h}{\partial x}(x_i, F_i), H_i = \frac{\partial h}{\partial F}(x_i, F_i).$$

And $f(x_i, F_i, u_i)$ represents the function value of $f(x, F, u)$ at the point (x_i, F_i, u_i). Similarly, $h(x_i, F_i)$ represents the function value of $h(x, F)$ at the point (x_i, F_i, u_i). These values are zero when the gas turbine is operating in a steady state condition and non-zero during a transition condition.

Eq. (10) can be rewritten as Eq. (11):

$$\begin{aligned} \dot{x} &= L_i x + \begin{bmatrix} M_i & N_i \end{bmatrix} \begin{bmatrix} F \\ u \end{bmatrix} + d_i \\ y &= E_i x + \begin{bmatrix} H_i & 0 \end{bmatrix} \begin{bmatrix} F \\ u \end{bmatrix} + e_i \end{aligned} \tag{11}$$

where,

$$d_i = f(x_i, F_i, u_i) - L_i x_i - M_i F_i - N_i u_i$$
$$e_i = h(x_i, F_i) - E_i x_i - H_i F_i.$$

Therefore, the Jacobian matrixes are as follow:

$$A = L_i, B = \begin{bmatrix} M_i & N_i \end{bmatrix}, C = E_i, D = \begin{bmatrix} H_i & 0 \end{bmatrix}.$$

The Jacobian matrixes are dynamic matrixes and change with the operating condition of gas turbine. The elements in the matrixes are determined by the parameters of the gas turbine nonlinear model. Thus, if the generalized expressions of the Jacobian matrix are determined, it is possible to determine the Jacobian matrix quickly based on the current parameters of the nonlinear model.

4.2 Jacobian matrix

Fig. 3 shows the decomposed modules and the information flows of the nonlinear model. As shown in this figure, the models of the main component are decomposed into several sub-modules, and each sub-module includes a nonlinear equation. For instance, the model of the compressor is decomposed into the temperature sub-module, the corrected mass flow sub-module and the isentropic efficiency sub-module. Linearized each sub-module, the linearization model of the component can be derived by symbolic computation according to the information flows between sub-modules. Then, the generalized expression of the Jacobian matrix can be derived by linearization of the nonlinear model. In this paper, the derivation of the Jacobian matrix at a non-equilibrium point is briefly described below.

The analytic linearization method can only be directly performed on the expression, but for the gas turbine nonlinear model, the component map cannot be presented as an expression instead of as a look-up table. But the mass flow can be

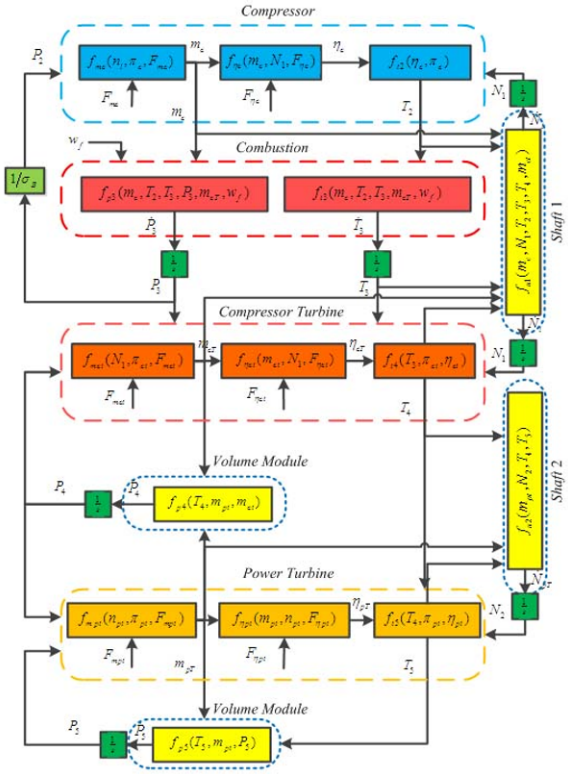

Fig. 3. Modules and the information flow of the gas turbine nonlinear mathematical model.

expressed as a function of rotational speed and pressure ratio (Namely, $m = f(N, \pi)$) and the efficiency can be expressed as a function of mass flow and rotational speed (Namely, $\eta = f(m, N)$). In addition, the mass flow and the efficiency will be changed when the fault occurs; in other words, the mass flow and the efficiency can also be expressed as a function of the fault factors. Hence, the mass flow and the efficiency sub-modules can be expressed as Eq. (12).

$$\begin{cases} m = f_m(N, \pi, F_m) \\ \eta = f_\eta(m, N, F_\eta). \end{cases} \tag{12}$$

Linearized Eq. (12) by using the central difference method, as shown in Eq. (13).

$$\begin{cases} m = D_m u_m + m_i - D_m u_{mi} \\ \eta = D_\eta u_\eta + \eta_i - D_\eta u_{\eta i} \end{cases} \tag{13}$$

where D_m, D_η denote the linearization matrix, and $u_m = [N\ \pi\ F_m]^T$, $u_\eta = [m\ N\ F_\eta]^T$, $u_{mi} = [N_i\ \pi_i\ F_{mi}]^T$, $u_{\eta i} = [N_i\ \pi_i\ F_{mi}]^T$.

The other sub-modules shown in Fig. 3 can be directly linearized. The component linear model can be derived according the relationship between the sub-modules that form the component model by using symbolic computation. Finally, the nonlinear equation shown in Eq. (1) can be linearized, and the intermediate variable of the equation can be eliminated ac-

cording to the relationship between the components as shown in Fig. 3. The analytic linearization equation of Eq. (1) at arbitrary point is shown in Eq. (14).

$$\begin{aligned}
\dot{T}_3 &= A_{t3}T_3 + B_{t3}u_{t3} + \dot{T}_{3i} - A_{t3}T_{3i} - B_{t3}u_{t3i} \\
\dot{P}_3 &= A_{p3}P_3 + B_{p3}u_{p3} + \dot{P}_{3i} - A_{p3}P_{3i} - B_{p3}u_{p3i} \\
\dot{P}_4 &= B_{p4}u_{p4} + \dot{P}_{4i} - B_{p4}u_{p4i} \\
\dot{P}_5 &= A_{p5}P_5 + B_{p5}u_{p5} + \dot{P}_{5i} - A_{p5}P_{5i} + B_{p5}u_{p5i} \\
\dot{N}_l &= A_{nl}n_l + B_{nl}u_{nl} + \dot{N}_{li} - A_{nl}n_{li} + B_{nl}u_{nli} \\
\dot{N}_P &= A_{np}n_p + B_{np}u_{np} + \dot{N}_{Pi} - A_{np}n_{pi} + B_{np}u_{npi}
\end{aligned} \tag{14}$$

where u contains state variables, fault factors and control variables. Rewriting Eq. (14) as a state space model, the variables are divided into two sets, one set of state variables and one set of fault factors and a control variable. In this paper, there are six state variables, and the control variables are the fuel flow and the six fault factors. Similarly, according to Fig. 3, the linearization equation of the measurement parameters can be derived by the analytic linearization method. Thus, the analytic expression as shown in Eq. (11) can be obtained. The analytic linearization process indicates that the analytic expression of the Jacobian matrix does not change with the operating conditions, but the Jacobian matrix will vary with the operating conditions because it is a function of the gas turbine parameters.

It is important to note that the proposed Jacobian matrix determination approach needs to call the engine nonlinear model only once in each step, and then, the Jacobian matrix can be obtained according the analytic expression. Traditional approaches, such as the perturbation method, need to call the engine nonlinear model 14 times to obtain the perturbations and then used to generate the Jacobian matrix [23]. Therefore, the computation cost of the proposed approach is less than that of the traditional approach and more suitable for on-line applications.

4.3 The model of the mode set

The effect of fault on the gas turbine measurement parameters is similar to the effect of the control variable. When the gas turbine is in the healthy condition, the fault factors are equal to one, namely, $F = 1_{6x1}$, and will change when the fault occurs. For example, when the compressor occurs a fault that causes a decrease in the corrected mass flow, then $F_{mc} < 1$, and the other fault factors remain 1. The gas turbine measurement parameters will deviate from the healthy condition, so these deviations may be considered as a result of the change in fault factors. Conversely, fault can be implanted into the healthy model by changing the fault factors. Considering the role of control variables, the fault factors were regarded as control variables in this paper. By changing the value of the fault factors, it can control the healthy model to become the corresponding faulty model. Therefore, as shown in Eq. (15), the fault factors are considered as the control variables, and different fault models can be obtained by changing the fault factors which control the healthy model. Finally, the model of the mode set is:

$$\begin{aligned}
\dot{x} &= f(x,[\underbrace{\sum_{j=1}^{q} b_j z_j}_{control\ variable},u]) \\
y &= h(x,[\sum_{j=1}^{q} b_j z_j,0])
\end{aligned} \tag{15}$$

where u denotes the real control variable, namely w_f, $\sum_{j=1}^{q} b_j z_j$ denotes the virtual control variables consisting of the fault factors, q represents the number of possible faults in the gas turbine. In this paper, the value is 6. b_j represents the fault severity of the *j-th* fault, and it is a scalar. z_j is a 6×1 vector representing the location of the fault. When a fault occurs, the value of the corresponding element in z_j is 1, and the value of other elements is 0. In addition, when the gas turbine is in a healthy condition, $\sum_{j=1}^{q} b_j z_j$ is a 6×1 unit vector, and it is a 6×1 nonzero vector in the event of a fault. Therefore, the mode set that includes the healthy mode and the different faulty modes can be obtained from Eq. (15), and this will contribute to the automatic generation of the model set, which will be described in detail in Sec. 5.

5. Implementation of MM-based FDI approach

In this section, the hierarchical detection and isolation architecture was developed for both single and multiple faults in the gas turbine, and the automatic generation method of the mode set was proposed based on the non-equilibrium analytic linearization model.

5.1 Hierarchical detection and isolation architecture

In this paper, six component faults corresponding to the six fault factors mentioned in Table 1 were investigated. Hence, the total number of modes in the mode set is seven, where mode 1# corresponding to the healthy condition and modes 2# to 7# corresponding to the six different faulty conditions. The hierarchical architecture is shown in Fig. 4.

In this architecture, fault detection and isolation is divided into multiple levels, and each level is activated in sequence. The first level is the single fault detection and isolation level, assuming the gas turbine starts from the healthy condition. Thus, the mode set in this level has a healthy mode and the 6 different faulty modes correspond to 1 % decrease in each fault factor with respect to health condition. When starting to detect and isolate faults, only the first level is activated, and the other levels are deactivated. When a fault is detected and isolated, the algorithm will activate the next level and deactivate the previous level, and the mode set in the next level will be automatically generated according the result of the previous level. This will be described in detail in the next part.

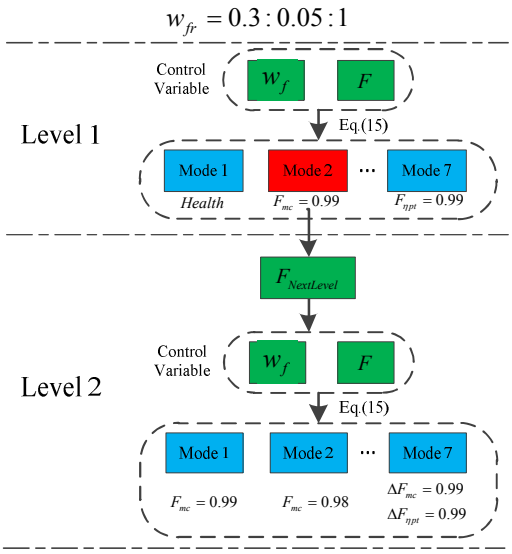

Fig. 4. Hierarchical detection and isolation architecture.

For instance, as shown in Fig. 4, if the compressor mass flow fault is detected and isolated in the first level, then the mode set of level 2 will be obtained according the result, and mode 1# corresponds to the compressor mass flow fault with a 1 % decrease, while mode 2# corresponds to a compressor mass flow fault with more severity, considering a 2 % decrease. Modes 3#-7# correspond to double concurrent faults, including a compressor mass flow fault with a 1 % decrease and one of the other different faults with a 1 % decrease. The mode set of the third level and the subsequent levels are obtained similar to level 2.

5.2 Mode set automatic generation method

In this section, an online automatic generation method is proposed, and the online automatic generation of the seven modes in the model set is described in detail.

Table 4 shows the possible fault modes in level 1 and level 2 of the hierarchical architecture [15]. In level 1, there are only 7 modes, but in level 2, there are 42 modes, mainly classified into 6 sets, with each set corresponding to one of the possible detection and isolation results. For instance, if the compressor mass flow fault is detected and isolated in level 1, then the first set will be selected as the mode set of level 2. However, the kind of fault occurs cannot be known before it is isolated, so all possible modes need to be obtained in advance. And then, the modes are chosen according to the result of the previous level. However, the number of the possible modes is too large to practical application. Therefore, in this paper, an online automatic generation method was proposed to overcome the problem mentioned above. In this method, when a fault is detected and isolated, the matrix $\sum_{j=1}^{q} b_j z_j$ which consisting of the fault factors defined in Eq. (15) will be known, and the new matrix corresponding to the next level can be calculated based on the previous level. Then, the mode set of the next level can be obtained based on the healthy mode through the control of the new matrix consisting of fault factors.

Therefore, to generate the mode set in the next level is mainly to obtain the matrix $\sum_{j=1}^{q} b_j z_j$ in the next level. The proposed on-line automatic generation algorithm is shown in Table 5. This algorithm first determines the number and location of the fault modes that occurred in the previous level according to the results, namely, the hypothesis conditional probability vector $p_{upper\ level}$ and the matrix $F_{upper\ level}$. For the hypothesis conditional probability vector, a threshold is selected to determine the occurrence of the fault. Then, the ma-

Table 4. Operating modes corresponding to various possible two concurrent scenarios.

Levels	Operating modes						
	1#	2#	3#	4#	5#	6#	7#
Level 1	P1	P2	P3	P4	P5	P6	P7
Level 2	P2	P2 (2 %)	P2 P3	P2 P4	P2 P5	P2 P6	P2 P7
	P3	P3 P2	P3 (2 %)	P3 P4	P3 P5	P3 P6	P3 P7
	P4	P4 P2	P4 P3	P4 (2 %)	P4 P5	P4 P6	P4 P7
	P5	P5 P2	P5 P3	P5 P4	P5 (2 %)	P5 P6	P5 P7
	P6	P6 P2	P6 P3	P6 P4	P6 P5	P6 (2 %)	P6 P7
	P7	P7 P2	P7 P3	P7 P4	P7 P5	P7 P6	P7 (2 %)

Table 5. Mode set automatic generation algorithm.

Step 1: Determine the type and number of the current faults

$m_i = find(p_{upper\ level} > 0.98)$

$z_i = find(F_{upper\ level}(:, m_i) < 1)$

$n = numel(z_i)$

Step 2: Generating the fault factors matrix $\Delta F_{next\ level}$ of the next level

for k=1:n

$F_{next\ level}(z_i(k), :) = F_{upper\ level}(z_i(k), m_i);$

$F_{next\ level}(z_i(k), z_i(k)+1) = F_{upper\ level}(z_i(k), m_i) - s_i;$

end

Step 3: Automatic generate the mode set of the next level according the Eq. (15)

$$\dot{x} = f(x, [\sum_{j=1}^{q} b_j z_j, u])$$

$$y = h(x, [\sum_{j=1}^{q} b_j z_j, 0])$$

Notation

$p_{upper\ level}$ denotes the hypothesis conditional probability matrix of the 7 modes in the previous level, a 7x1matrix;
$F_{upper\ level}$ denotes the fault factors matrix of the next level, a 6x7matrix;
$F_{next\ level}$ denotes the fault factors matrix of the previous level, a 6x7 matrix
s_i denotes the increased severity in the next level, a scalar. $s_i = 0.01$ in this paper.

trix of the next level, $F_{next\ level}$, is obtained. Finally, this matrix will be implanted in Eq. (15), and the seven possible fault modes will be obtained based on the healthy model through the control of the matrix to realize the automatic generation of the model set. With this algorithm, the mode set of each level can be automatically generated according to the results of the previous level and does not need to be obtained in advance. In this paper, it is assumed that the severity of the fault increases with the activated level of the hierarchical architecture and the severity of each fault is equivalent to the decrease of fault factors. In this paper, assuming the fault factors decrease by s_i each time, namely, 0.01.

5.3 Case study description

To verify the effectiveness of the proposed approach, the nonlinear MM-based FDI approach, which based on the STEKF, was developed for detection and isolation of both single and multiple faults of a two-shaft marine gas turbine in the simulation environment. The performance of the approach was analysed in different fault scenarios and conditions. In addition, the effects of Q and R on the MM-based FDI approach performance were also investigated. Therefore, three cases were mainly investigated in this paper.

The first case mainly focuses on the detection and isolation of single fault with different severities under steady state condition and transient condition. In this case, the detection factor and the isolation factor were introduced to evaluates the performance of the proposed MM-based FDI approach.

The second case mainly focuses on the fault detection and isolation of multiple faults with different severities under a steady state condition. It is assumed that a compressor mass flow fault with a 1 % decrease and a compressor turbine mass flow fault with a 2 % decrease occur in the gas turbine, and the results of the fault detection and isolation were analysed.

The third case mainly focuses on investigating the effects of 0.1*Q and 0.1*R on the performance of the proposed MM-based FDI approach.

In this paper, it is assumed that, during the detection and isolation of multiple faults, the time between the occurrences of faults is sufficient for the MM-based FDI algorithm to detect and isolate the first fault. The analysis and discussions of the results are presented in the following section, and all these results were compared with that of the traditional EKF-based MM approach.

6. Simulation results and analysis

In this section, the results of the case studies mentioned in the previous section were analysed and discussed. In this paper, it is assumed that the initial condition of the gas turbine is in healthy condition, it means that the initial value of the hypothesis conditional probability of the mode that corresponds to the healthy condition is 1, while the initial value of the hypothesis conditional probability of other modes is 0.

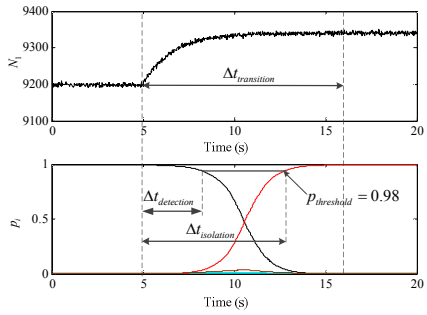

Fig. 5. Schematic of the detection threshold, the detection time, the isolation time and the transient time.

Considering the poor tracking ability of the Kalman filter for the mutation condition and to avoid the problem that the hypothesis conditional probability of the mode is close to 0 and changes slowly when the fault occurs in this paper, a minimum hypothesis conditional probability of 0.001 was set for each mode.

6.1 Fault detection and isolation factors

To detect and isolate faults, the detection and isolation threshold $p_{threshold}$ was introduced. The detection threshold is used to indicate that the current condition has changed when the probability of the current mode decreases to the threshold. The isolation threshold is used to indicate that the current condition is ensured when the probability of a new mode increases to the threshold. In this paper, it is assumed that the detection threshold equals the isolation threshold, and the threshold value is 0.98, as shown in Fig. 5. The detection and isolation threshold in this paper is only used for determining the fault detection and isolation time, and it does not affect the false alarm and the missing alarm.

In addition, to analyse the detection and isolation performance of the proposed approach, the detection factor (f_d) and isolation factor (f_i) were introduced. They are defined as the ratios of the detection time and isolation time to the transient time caused by the fault, respectively. When the value of the factor is greater than 1, it means that the detection time or the isolation time is greater than the transition time caused by the fault. It indicates the fault can be detected and isolated, but not in real time. When the value is less than 1, it indicates that the fault can be detected or isolated in real time. The defined detection and isolation factors are shown in Eq. (16), and Fig. 5 shows schematic of the detection time, isolation time, and transient time.

$$\begin{cases} f_d = \Delta t_{\text{detection}} / \Delta t_{transition} \\ f_i = \Delta t_{isolation} / \Delta t_{transition}. \end{cases} \tag{16}$$

6.2 Single fault detection and isolation

In this case, the detection and isolation of a single fault with different severities in the two-shaft marine gas turbine under

steady state and transient conditions were investigated. The six faults mentioned in Sec. 2 were detected and isolated by using the proposed STEKF-based MM approach and compared with the results of traditional EKF-based MM approach. In this case, the severities of the injected fault include 1 %, 3 % and 5 % decreases, and all faults occur at t = 5 s. Table 6 shows the detection time, isolation time, and transition time of both the proposed approach and the traditional approach.

Table 6 shows that, for single fault detection and isolation, with the fault severity increase, the detection time and the isolation time will decrease. This is mainly due to the more obvious difference between modes that with more serious fault, resulting in a faster change in the hypothesis conditional probability of these modes. Comparing the detection time and the isolation time of the two approaches, it can be seen that both approaches can detect and isolate the fault accurately, and the detection time and the isolation time of the proposed approach are shorter than the traditional approach. Fig. 6 shows the detection and isolation results when injecting a 1 % decrease in each fault factor at t = 5 s, corresponding to the first row of each mode in Table 6. It needs to mention that the p_i in the Fig. 6 and the subsequent figures indicates the hypothesis conditional probability of each mode which is defined by Eq. (6).

Fig. 7 shows the detection factor and the isolation factor of both approaches for each fault with different severities. The figure shows that the detection and isolation factors in both approaches decrease rapidly with increase in the severity of fault. It indicates that fault detection and isolation is easier for a more serious fault. In addition, as seen from Fig. 7, both the detection factor and the isolation factor for single fault detection and isolation are less than 1, indicating that these faults can be detected and isolated in real time.

To evaluate the performance of the proposed approach in transient condition, the fault injected during the transient condition was investigated. In this case, the relative fuel flow decreases linearly from 1 at t = 5 s to 0.8 at t = 25 s, while the compressor mass flow fault with 1 % decrease is injected at t = 15 s, and the result shows in the Fig. 8. The figure shows that the proposed approach can still detect and isolate the fault

Table 6. The detection and isolation time of the STEKF and the EKF.

Fault mode	Severity	t_{dEKF}	t_{dSTF}	t_{iEKF}	t_{iSTF}	t_{tr}
Mode 2	1	6.60	6.34	8.86	8.64	17.00
	3	5.26	5.22	5.50	5.50	18.36
	5	5.16	5.12	5.26	5.24	18.76
Mode 3	1	5.92	5.42	6.96	5.96	13.98
	3	5.14	5.08	5.28	5.16	15.48
	5	5.08	5.06	5.16	5.08	16.94
Mode 4	1	7.84	7.64	12.12	11.90	16.02
	3	5.44	5.34	5.84	5.84	17.04
	5	5.24	5.12	5.46	5.28	16.54
Mode 5	1	6.44	5.82	8.28	7.38	14.28
	3	5.18	5.08	5.50	7.30	16.22
	5	5.08	5.06	5.20	6.18	13.52
Mode 6	1	9.84	9.02	16.74	15.54	17.76
	3	5.70	5.56	6.44	7.76	14.88
	5	5.36	5.18	5.64	6.14	15.84
Mode 7	1	5.78	5.40	7.16	6.22	15.84
	3	5.10	5.06	5.28	5.14	12.76
	5	5.06	5.04	5.12	5.08	13.60

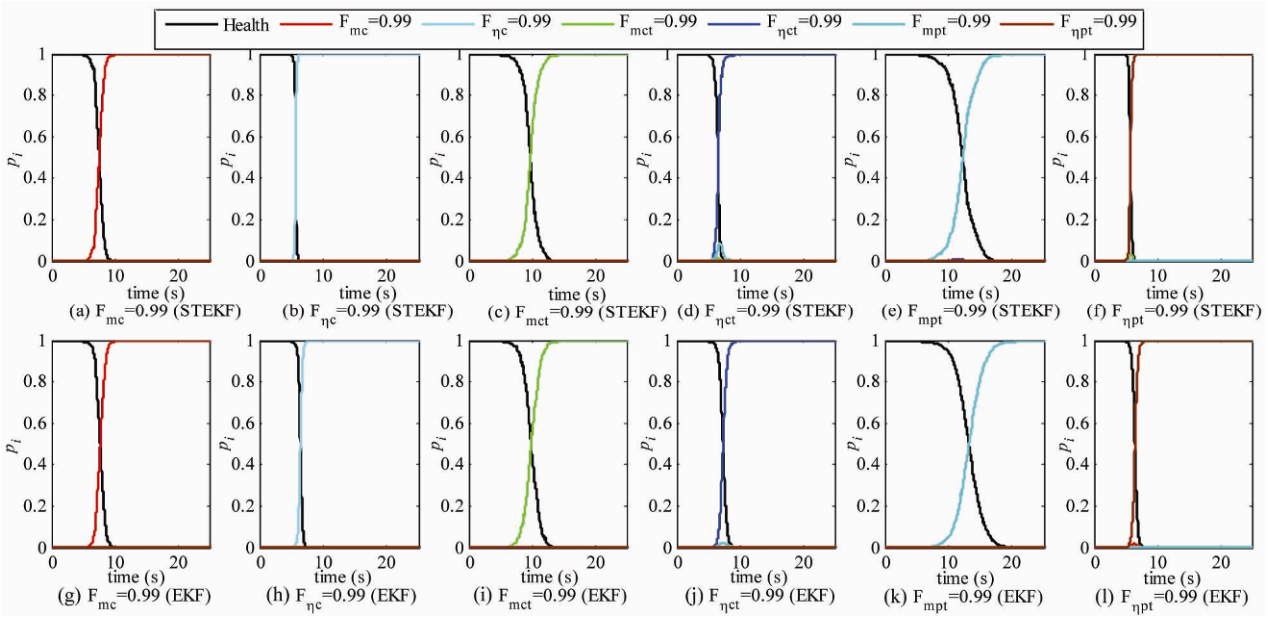

Fig. 6. The detection and isolation results of the STEKF based multiple model approach and the EKF based multiple model approach when injected each fault with 1 % decrease.

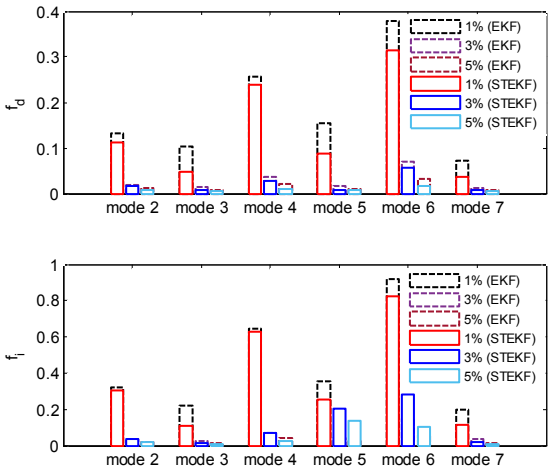

Fig. 7. The detection factor and isolation factor of the STEKF based multiple model approach and the EKF based multiple model approach.

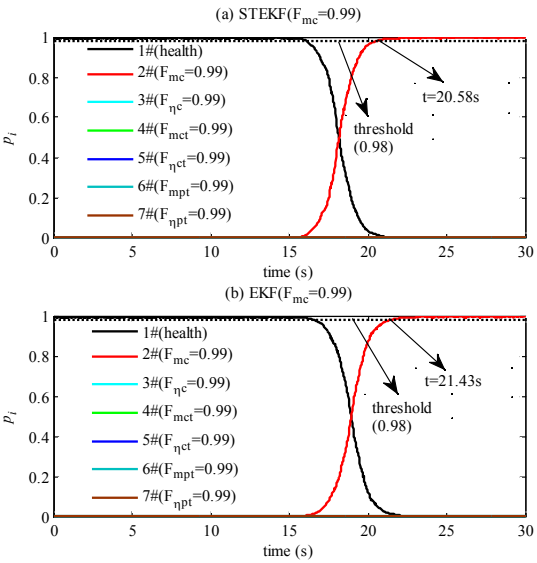

Fig. 8. The detection and isolation results of the STEKF-based MM approach and the EKF-based MM approach under transition condition.

accurately under a transition condition, but the detection and isolation time is longer than that under a steady state condition. In addition, the detection and isolation time of the proposed approach is shorter than the traditional approach.

6.3 Multiple faults detection and isolation

In this case, multiple fault detection and isolation was studied by using the proposed approach and compared with the results of the traditional approach. Suppose the faults do not occur simultaneously and the time intervals between the faults are sufficient for the MM-based FDI algorithm to detect and isolate the first fault. In this paper, assume that a 1 % decrease in the compressor mass flow is injected at t = 5 s and a 2 % decrease in the compressor turbine mass flow is injected at t = 25 s. The MM-based FDI approach based on the hierarchical

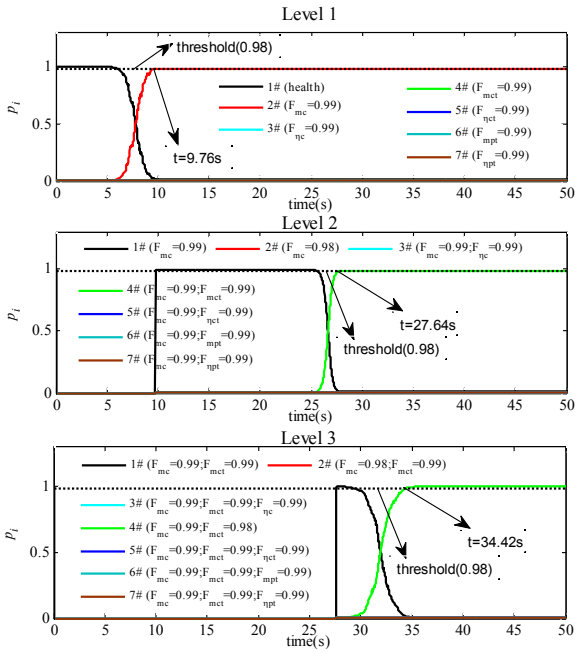

Fig. 9. Multiple faults detection and isolation results of the proposed STEKF-based MM approach under steady state condition.

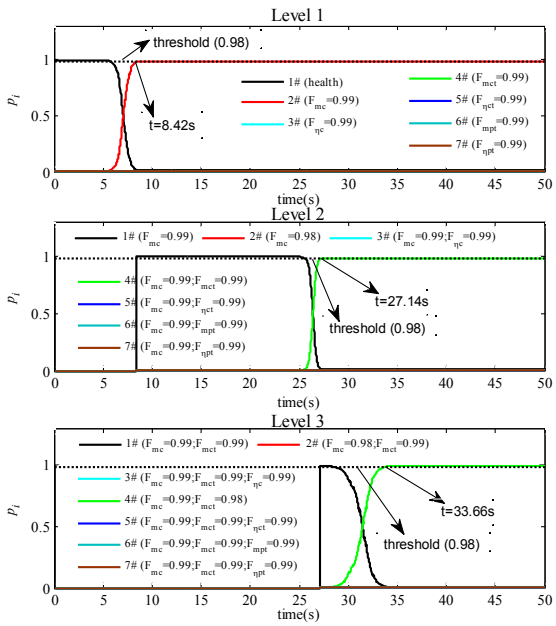

Fig. 10. Multiple faults detection and isolation results of the EKF-based MM approach under steady state condition.

architecture described in Sec. 5 was developed to detect and isolate the multiple faults. The hypothesis conditional probabilities of each mode in different levels of the two approaches are shown in Figs. 9 and 10, respectively.

Figs. 9 and 10 show that, for the first fault, the detection and isolation time is the same as in single fault detection and isolation. For the second fault, although both approaches can accurately detect and isolate the fault, the proposed approach has a slightly longer detection and isolation time than the traditional

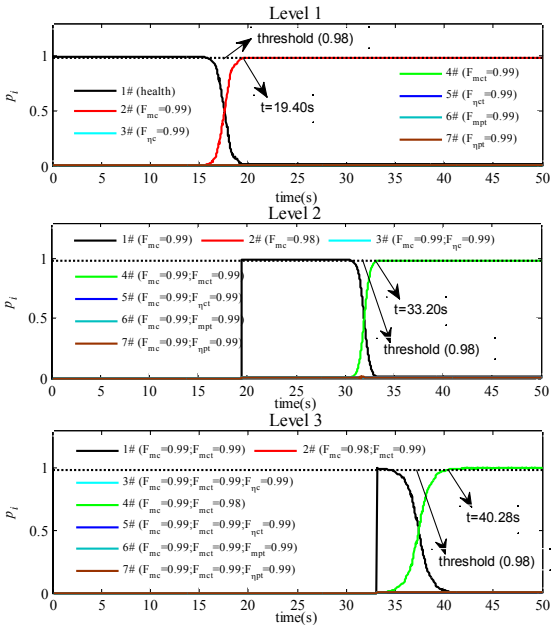

Fig. 11. Multiple faults detection and isolation results of the proposed STEKF-based MM approach under transition condition.

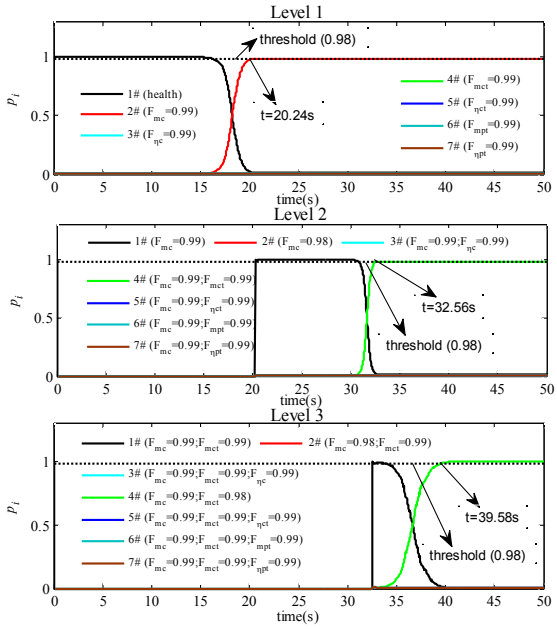

Fig. 12. Multiple faults detection and isolation results of the EKF-based MM approach under transition condition.

method. In addition, the proposed mode set automatic generation method can generate the mode set of the next level according to the detection and isolation results of the previous level. Thus, each level can maintain seven possible modes, which greatly reduces the computational cost.

Similarly, for the above described multiple faults, the proposed approach and the traditional approach were used to detect and isolate the faults under a transient condition. In this case, the relative fuel flow starts to decrease linearly from 1 at t = 5 s and decreases to 0.8 at t = 40 s, while the first fault is injected at t = 15 s, and the second fault is injected at t = 30 s. The results for detection and isolation by two approaches are presented in Figs. 11 and 12. These figures show that the two approaches can still accurately detect and isolate the injected faults. However, the detection and isolation time required by two approaches are longer than that under steady state conditions, and the time taken by the proposed approach to detect and isolate the second fault is longer than that of the traditional approach.

As seen from the above results for single and multiple fault detection and isolation, the performance of the proposed multiple model approach based on STEKF is similar to that of the traditional multiple model approach based on the EKF in single fault detection and isolation. However, for multiple fault detection and isolation, the detection time and the isolation time of the proposed multiple model approach based on STEKF is slightly longer than that of the traditional approach, especially for detecting and isolating the second fault.

6.4 Effect of model uncertainty on fault detection and isolation

In this section, the effect of model uncertainty on the performance of the nonlinear multiple model fault detection and isolation approaches was investigated. In this case, the influence factors that cause model uncertainty in the performance of the fault detection and isolation algorithm were studied, such as the inaccuracy of the system noise covariance Q and the inaccuracy of the measurement noise covariance R. The results of single fault detection and isolation show that with the fault severity increase, the differences between these modes that represent the possible operating conditions of the gas turbine will more significant, and the fault will be easier to detect and isolate. In other words, fault detection and isolation is more difficult for the injected fault with 1 % decrease than the fault with 3 % and 5 % decrease. Therefore, a fault with 1 % decrease was selected in this section to investigate the effect of model uncertainty on the performance of the fault detection and isolation algorithm and to compare the robustness of the STEKF-based MM approach to model uncertainty with that of the EKF-based MM approach.

6.4.1 Effect of system noise covariance Q

In this section, the effect of model uncertainty caused by the inaccuracy of the initial system noise covariance Q on the performance of the two algorithms was investigated. In this case, by artificially reduce the system noise covariance to 0.1*Q, and the other parameters remain unchanged. The severities of the injected fault are decreased by 1 %, and each fault occurs at t = 5 s. The results of detect and isolate the injected fault by using the proposed STEKF-based MM approach and the traditional EKF-based MM approach are presented in Fig. 13.

As seen from the figure, the approach proposed in this paper can still accurately detect and isolate the injected faults

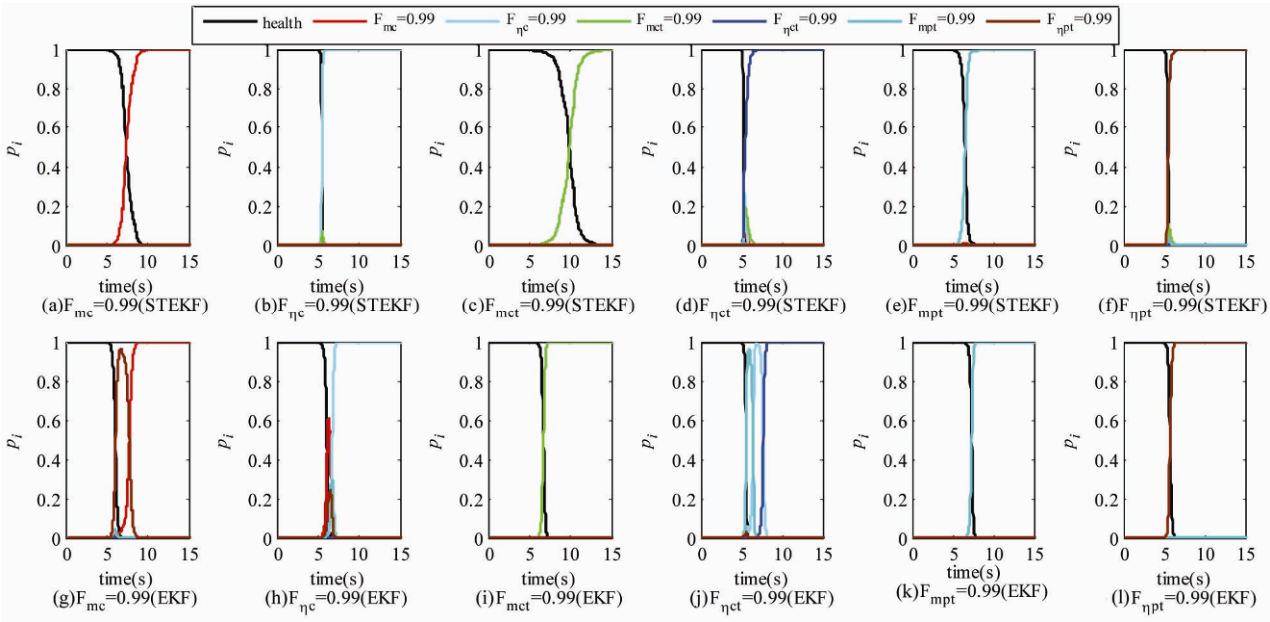

Fig. 13. The detection and isolation results of two approaches when the initial system noise covariance is 0.1*Q.

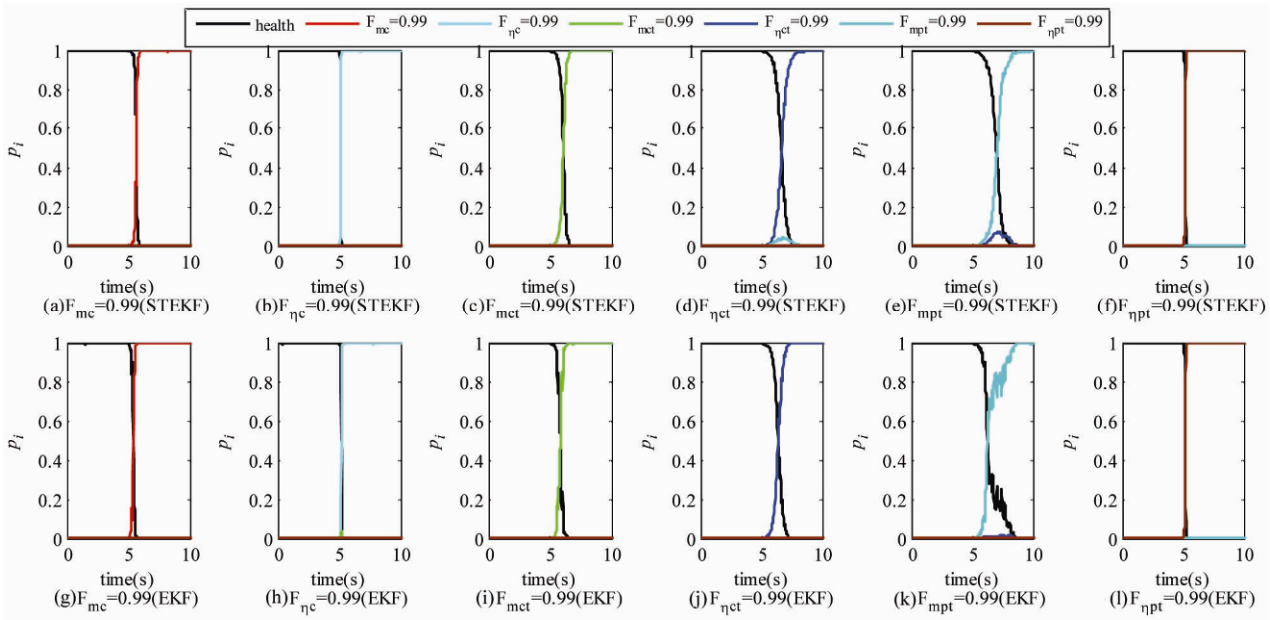

Fig. 14. The detection and isolation results of two approaches when the initial system noise covariance is 0.1*R.

even when the initial noise covariance of the system is inaccurate. In contrast to the case corresponding to Fig. 6, the detection and isolation time of all modes except the compressor turbine efficiency fault are increase, and for the compressor turbine efficiency fault, the probability of other modes will varying but does not influence the isolation result. For the multiple model fault detection and isolation approach based on the EKF, although the injected fault eventually can be accurately detected and isolated, but for the compressor mass flow fault, the hypothesis conditional probability of the mode corresponding to the power turbine efficiency fault will increase and may lead to incorrect fault isolation. In addition, when a compressor turbine efficiency fault is injected, the probability of the mode corresponding to the compressor efficiency fault will increase to greater than 0.98, which may cause a false alarm. By comparing the detection and isolation results of the two methods, it indicates that the proposed method has better robustness to the model uncertainty caused by the inaccuracy of initial system noise covariance.

6.4.2 Effect of sensor noise covariance R

The effect of the model uncertainty caused by the inaccuracy of the initial sensor noise covariance R on the performance of the two approaches was studied. In this case, by artificially reduce the sensor noise covariance to 0.1**R*, and the other parameters remain unchanged. Consequently, the severities of the injected fault are decreased 1 %, and each fault occurs at t = 5 s. The fault detection and isolation results of the two approaches are shown in Fig. 14.

As seen from the figure, the approach proposed in this paper can accurately detect and isolate the injected fault, but the detection and isolation time is increased than the case corresponding to Fig. 6. For the traditional multiple model approach based on the EKF, when the initial sensor noise covariance decreased to 0.1**R*, the hypothesis conditional probability of each mode fluctuated during detection and isolation process, especially for the power turbine mass flow fault. This is mainly due to the poor robustness of the EKF to model uncertainties, whereas the robustness of the STEKF to model uncertainty makes the detection and isolation results less affected.

7. Conclusion

In this paper, the gas turbine nonlinear fault detection and isolation approach based on multiple models was studied. An improved STEKF-based MM approach was proposed to overcome the shortcoming of poor robustness to model uncertainty of the traditional EKF-based MM approach, and to keep the filter residuals follow Gaussian distribution to satisfy the Gaussian density function. In addition, a mode set automatic generation method was also proposed in this paper, in which the mode set of the current level will be automatically generated according to the results of the previous level. The approach proposed in this paper was applied to fault detection and isolation of a two-shaft marine gas turbine engine and compared with the results of traditional EKF-based MM approach. The results show that the performance of the approach proposed in this paper and that of the traditional approach are similar for single fault detection and isolation, and in multiple fault detection and isolation, although the detection time and the isolation time of the proposed approach are slightly longer than that of the traditional approach, but it more robust to mode uncertainty than the traditional approach.

Acknowledgments

This research is supported by the Fundamental Research Funds for the Central Universities (HEUCFP201722).

Reference

[1] A. J. Volponi, Gas turbine engine health management: Past, present and future trends, *Journal of Engineering for Gas Turbines & Power,* 58 (136) (2013) 433-455.

[2] M. Tahan, M. Muhammad and Z. A. A. Karim, Performance evaluation of a twin-shaft gas turbine engine in mechanical drive service, *Journal of Mechanical Science & Technology*, 31 (2) (2017) 937-948.

[3] R. Isermann, *Fault diagnosis systems: An introduction from fault detection to fault tolerance,* Springer Verlag, Berlin (2005).

[4] L. Marinai, D. Probert and R. Singh, Prospects for aero gas-turbine diagnostics: A review, *Applied Energy,* 79 (1) (2004) 109-126.

[5] K. Mathioudakis, Comparison of linear and nonlinear gas turbine performance diagnostics, *Journal of Engineering for Gas Turbines & Power,* 127 (1) (2003) 451-459.

[6] M. Amozegar and K. Khorasani, An ensemble of dynamic neural network identifiers for fault detection and isolation of gas turbine engines, *Neural Networks the Official Journal of the International Neural Network Society,* 76 (2016) 106-121.

[7] R. Ganguli, Fuzzy logic intelligent system for gas turbine module and system fault isolation, *Journal of Propulsion & Power*, 18 (2) (2002) 440-447.

[8] T. Kobayashi and D. L. Simon, *Aircraft engine sensor/actuator/component fault diagnosis using a bank of Kalman filters*, NASA: Houston, TX, USA, March (2003).

[9] T. Kobayashi and D. L. Simon, *Application of a bank of Kalman filters for aircraft engine fault diagnostics*, American Society of Mechanical Engineers (2003) 461-470.

[10] T. Kobayashi and D. L. Simon, *Hybrid Kalman filter: A new approach for aircraft engine in-flight diagnostics*, NASA/TM—2006-214491.

[11] M. E. Orchard and G. J. Vachtsevanos, A particle filtering-based framework for real-time fault diagnosis and failure prognosis in a turbine engine, *Mediterranean Conference on Control & Automation*, *MED '07* (2007) 1-6.

[12] T. E. Menke and P. S. Maybeck, Sensor/actuator failure detection in the Vista F-16 by multiple model adaptive estimation, *IEEE Transactions on Aerospace & Electronic Systems,* 31 (4) (1995) 3135-3141.

[13] P. D. Hanlon and P. S. Maybeck, Multiple-model adaptive estimation using a residual correlation Kalman filter bank, *IEEE Transactions on Aerospace & Electronic Systems*, 36 (2) (2000) 393-406.

[14] N. Meskin, E. Naderi and K. Khorasani, A multiple model-based approach for fault diagnosis of jet engines, *IEEE Transactions on Control Systems Technology*, 21 (1) (2013) 254-262.

[15] N. Meskin, K. Khorasani and E. Naderi, Nonlinear fault diagnosis of jet engines by using a multiple model-based approach, *Journal of Engineering for Gas Turbines & Power,* 13 (1) (2011) 63-75.

[16] D. H. Zhou and P. M. Frank, Strong tracking Kalman filtering of nonlinear time-varying stochastic systems with coloured noise: application to parameter estimation and

empirical robustness analysis, *International Journal of Control,* 65 (2) (1996) 295-307.

[17] Q. Yang, S. Li and Y. Cao, A new component map generation method for gas turbine adaptation performance simulation, *Journal of Mechanical Science and Technology*, 31 (4) (2017) 1947-1957.

[18] E. Tsoutsanis, N. Meskin, M. Benammar and K. Khorasani, Dynamic performance simulation of an aeroderivative gas turbine using the matlab simulink environment, *ASME 2013 International Mechanical Engineering Congress and Exposition* (2013) V04AT04A050.

[19] H. Rashidzadeh, S. M. Hosseinalipour and A. Mohammadzadeh, The SGT-600 industrial twin-shaft gas turbine modeling for mechanical drive applications at the steady state conditions, *Journal of Mechanical Science & Technology*, 29 (10) (2015) 4473-4481.

[20] J. H. Kim, S. K. Tong and S. J. Moon, Development of a program for transient behavior simulation of heavy-duty gas turbines, *Journal of Mechanical Science & Technology*, 30 (12) (2016) 5817-5828.

[21] P. Maybeck, Multiple model adaptive algorithms for detecting and compensating sensor and actuator/surface failures in aircraft flight control systems, *Int. J. Robust Nonlinear Control*, 9 (14) (1999) 1051-1070.

[22] T. A. Johansen, K. J. Hunt, P. J. Gawthrop and H. Fritz, Off-equilibrium linearisation and design of gain-scheduled control with application to vehicle speed control, *Control Engineering Practice*, 6 (2) (1998) 167-180.

[23] S. Dan, A comparison of filtering approaches for aircraft engine health estimation, *Aerospace Science & Technology,* 12 (4) (2008) 276-284.

Qingcai Yang received his B.S. degree in Harbin Engineering University in 2013. He is currently a graduate student for Ph.D. degree of Power and Energy Engineering at Harbin Engineering University. Mr. Yang's research interests are in the area of gas turbine performance simulation, gas turbine health estimation and gas path fault diagnosis.

Shuying Li received the B.S., M.S. and Ph.D. degrees in marine engineering, all from Harbin Engineering University in 1986, 1992 and 2000. She is a Professor of College of Power and Energy Engineering at Harbin Engineering University, China. Her research interests are in the areas of marine power plant performance and its control strategy, gas turbine engine fault diagnosis, advance measurement and testing.

Yunpeng Cao received the B.S. degree in Thermal Power Engineering from Hebei University of Technology in 2002, and the M.S., Ph.D. degrees in Marine Engineering, all from Harbin Engineering University in 2005, 2011. He is a Lecture of College of Power and Energy Engineering at Harbin Engineering University, China. His research interests are in the areas of marine power plant fault diagnosis and safety validation.